

# Statefinder hierarchy model for the Barrow holographic dark energy

Vinod Kumar Bhardwaj<sup>1</sup>, Archana Dixit<sup>2</sup> and Anirudh Pradhan<sup>3</sup>

<sup>1,2,3</sup>Department of Mathematics, Institute of Applied Sciences and Humanities, GLA  
University,  
Mathura-281 406, Uttar Pradesh, India

<sup>1</sup>E-mail: dr.vinodbhardwaj@gmail.com

<sup>2</sup>E-mail: archana.dixit@gla.ac.in

<sup>3</sup>E-mail: pradhan.anirudh@gmail.com

## Abstract

In this paper, we have used the state finder hierarchy for Barrow holographic dark energy (BHDE) model in the system of the FLRW Universe. We apply two DE diagnostic tools to determine  $\Lambda$ BHDE model to have various estimations of  $\Delta$ . The first diagnostic tool is the state finder hierarchy in which we have studied  $S_3^{(1)}$   $S_4^{(1)}$ ,  $S_3^{(2)}$   $S_4^{(2)}$  and second is the composite null diagnostic (CND) in which the trajectories ( $S_3^{(1)} - \epsilon$ ), ( $S_4^{(1)} - \epsilon$ ), ( $S_3^{(2)} - \epsilon$ ), ( $S_4^{(2)} - \epsilon$ ) are discussed, where  $\epsilon$  is fractional growth parameter. The infrared cut-off here is taken from the Hubble horizon. Finally, together with the growth rate of matter perturbation, we plot the state finder hierarchy that determines a composite null diagnosis that can differentiate emerging dark energy from  $\Lambda$ CDM. In addition, the combination of the hierarchy of the state finder and the fractional growth parameter has been shown to be a useful tool for diagnosing BHDE, particularly for breaking the degeneracy with different parameter values of the model.

**Keywords** : FLRW Universe, BHDE, Hubble Horizon, State finder hierarchy

PACS: 98.80.-k

## 1 Introduction

The cosmological findings [1]- [4] have indicated that there is an accelerated expansion. The responsible cause behind this accelerated expansion is a miscellaneous element having exotic negative pressure termed as dark energy (DE). In this field, an enormous DE models are suggested for the conceivable existence of DE such as  $\Lambda$ CDM models, holographic dark energy (HDE) models [5]- [10], and the scalar-field models [11]- [16], etc. In the direction of modified gravity, various efforts have been made, for instance, the  $f(R)$  theories [16]- [18], the Dvali-Gabadadze-Porrati (DGP) braneworld model [19] etc. Amidst other prevailing theoretical perspectives, the least complicated amongst all is the  $\Lambda$ CDM model which is in good agreement with observations. The  $\Lambda$ CDM model normally suffers from many theoretical problems such as fine tuning and coincidence problems [20]- [23].

For clarifying the accelerating expansion of universe, the dark energy has been considered as most encouraging factor [20, 23–25]. A large number of models have been proposed on idea of dark energy, but DE is still assumed as mysterious causes [26]– [30]. Fundamentally, DE problem might be an issue of quantum gravity. It is normally accepted that the holographic principle (HP) [31, 32] is one of the fundamental principles in quantum gravity. In 2004, Li proposed the (HDE) model [33], which is the primary DE model inspired by the HP. This model is in generally excellent concurrence with recent observational data [34]– [40]. Recently, Nojiri et al. [41] proposed a HDE model in which they have established the unification of holographic inflation with holographic dark energy.

Motivated by the holographic fundamentals and utilizing different framework entropies, some new types of DE models were suggested such as, the Tsallis holographic dark energy (THDE) [42, 43], the Tsallis ageographic dark energy (TADE) [44] the Renyi holographic dark energy (RHDE) [45, 46], and the Sharma–Mittal holographic dark energy (SMHDE) model [47, 48]. Recently many authors shows a great interest in HDE models and explored in different context [49]– [54].

Now a day our main concern is the  $\Lambda$ CDM instead of DE models, because our observational analysis are based on  $\Lambda$ CDM. The  $\Lambda$ HDE models generally deal with two key parameters: dimensionless HDE parameter and fractional density of cosmological constant. Since they decide the dynamical nature of DE and the predetermination of universe. For the evaluation of the various DE models, two diagnostic tools are generally used. The first one is the state finder hierarchy [55, 56], which is a geometrical diagnostic tool and it is model independent. The second parameter is the fractional growth parameter (FGP)  $\epsilon$  [57, 58], which presents an independent scale diagnosis of the universe’s growth history. Additionally, a variation of the state finder hierarchy along with FGP, referred to as composite null diagnosis (CND) [56] is often used to diagnose DE models.

In this way a clearer diagnosis called as state finder hierarchy (SFH)  $S_n$  has been recently implemented in [59]. The  $O_m$  diagnostic and statefinders are connected to the derivative of scale factor  $a$  and the expansion rate  $H(z)$ . Now the composite null diagnosis (CND) is a helpful and beneficial technique to the state finder progressive system, where the fractional growth parameter  $\epsilon$  associated with the structure growth rate [57, 58]. In this model [60], the researchers developed Barrow holographic energy. Here the authors utilized the holographic principle in a cosmological structure and Barrow entropy rather than the popular Bekenstein-Hawking. BHDE is also an engaging and thought-provoking optional framework for quantitatively describing DE.

Barrow [62] has recently found the possibility that the surface of the black hole could have a complex structure down to arbitrarily tiny due to quantum-gravitational effects. The above potential impacts of the quantum-gravitational space time form on the horizon region would therefore prompt another black hole entropy relation, the basic concept of black hole thermodynamics. In particular

$$S_B = \left( \frac{B}{B_0} \right)^{1 + \frac{\Delta}{2}}. \quad (1)$$

Here  $B$  and  $B_0$  stand for the normal horizon area and the Planck area respectively. The new exponent  $\Delta$  is the quantum-gravitational deformation with bound as  $0 \leq \Delta \leq 1$  [60]– [65].

The value  $\Delta = 1$  gives to the most complex and fractal structure, while  $\Delta = 0$  relates to the easiest horizon structure. Here as a special case the standard Bekenstein-Hawking entropy is reestablished and the scenario of BHDE has been developed. The inequality  $\rho_D L^4 \leq S$ , is given by the standard HDE, where  $L$  stands for the horizon length under the assumption  $S \propto A \propto L^{-2}$  [66]. The Barrow holographic dark energy models have been explored and discussed by various researchers [67] - [70] in various other contexts. The above relationship results in some fascinating holographic and cosmological setup results [31, 44]. It should be noted that the above relationship offers the usual HDE for the special case of  $\Delta = 0$ , i.e.  $\rho_D \propto L^{-2}$ . Consequently, the BHDE is definitely a more general paradigm than the standard HDE scenario. We are concentrating here on the general ( $\Delta > 0$ ) scenario. We consider  $H^{-1}$  Hubble horizon (HH) as an IR cut-off ( $L$ ). The energy density of BHDE is expressed as

$$\rho_D = CH^{2-\Delta} \quad (2)$$

where  $C$  is an unknown parameter.

In the current research article, we are considering the fundamental geometry of the universe to be a spatially flat, homogeneous and isotropic space time. The Hubble horizon has been regarded as an effective IR cut-off to describe the continuing accelerated expansion of the universe [60, 61]. The objective of this research is to apply the diagnostic tools to differentiate between the BHDE models with various other values of  $\Delta$ . Here, we use the diagnostic tool of the state finder hierarchy for BHDE that achieves the value of the  $\Lambda$ CDM model and demonstrates consistency of the model for proper estimation of the parameters. It is worth mentioning here that we have also demonstrated DE's physical scenario by taking Barrow exponent  $\Delta > 1$ . We arrange the manuscript as follows: The BHDE model suggested in [60] and the basic field equations are added in Section 2. The state finder hierarchy are discussed in Sec. 3. We explore the fractional state finder diagnostic in Sec. 4. Growth rate perturbations are discussed in Sec. 5. Section 6 contains the conclusive statements, discussion and discourse.

## 2 Basic field equations

The construction of modified Friedman equations with the application of gravity-thermodynamic conjecture is discussed in this section with the use of entropy from Barrow [71]. The metric reads as for the flat FRW Universe

$$ds^2 = -dt^2 + a^2(t)(dr^2 + r^2 d\Omega^2), \quad (3)$$

where  $\Omega^2 = d\theta^2 + \sin^2 \theta d\phi^2$ ,  $t$  is the cosmic time and  $a(t)$  is the dimensionless scale factor normalized to unity at the present time i.e.  $a(t_0) = 1$ .

The Friedmann first field equation for BHDE is given as :

$$H^2 = \frac{1}{3}8\pi G(\rho_D + \rho_m), \quad (4)$$

where  $\rho_D$  and  $\rho_m$  read as the energy density of BHDE and matter and expressed as  $\Omega_D = \frac{8\pi\rho_D G}{3H^2}$  and  $\Omega_m = \frac{8\pi\rho_m G}{3H^2}$  respectively. The conservation laws for matter and BHDE are defined as:

$$\dot{\rho}_m + 3H\rho_m = 0, \dot{\rho}_D + 3H(p_D + \rho_D) = 0.$$

From Eq (2), we get

$$\dot{\rho}_D = \frac{3C}{2}(2 - \Delta)H^{2-\Delta} \left( \frac{\Delta\Omega_D}{(\Delta - 2)\Omega_D + 2} - 1 \right). \quad (5)$$

Now, using Eq (4), we obtain

$$\frac{\dot{H}}{H^2} = \frac{3}{2} \left( \frac{\Delta\Omega_D}{(\Delta - 2)\Omega_D + 2} - 1 \right). \quad (6)$$

Using Eq. (6), the deceleration parameter (DP)  $q$  is expressed by

$$q = -1 - \frac{\dot{H}}{H^2} = \frac{1 - (\Delta + 1)\Omega_D}{(\Delta - 2)\Omega_D + 2}. \quad (7)$$

By utilizing the Eqs. (5) and (6), we get the EoS parameter as:

$$\omega_D = -\frac{\Delta}{(\Delta - 2)\Omega_D + 2}. \quad (8)$$

From Eqs. (6) and (8), we derive  $\omega'_D$  as

$$\omega'_D = -\frac{3\Delta^3(\Omega_D - 1)\Omega_D}{((\Delta - 2)\Omega_D + 2)^3}, \quad (9)$$

where dash is the derivative with respect to  $\ln a$ . In similar way by the use of Eqs. (6) and (8), we obtain  $\Omega'_D$  as:

$$\Omega'_D = -\frac{3\Delta\Omega_D(\Omega_D - 1)}{(\Delta - 2)\Omega_D + 2}. \quad (10)$$

### 3 Statefinder hierarchy

Statefinder hierarchy [72–74] is an effective diagnosis of geometry. It is appropriated to discriminate, various DE models from the  $\Lambda$ CDM model by utilizes the higher order derivative of the scale factor. In this case, the scale factor  $a(t)$  is the main dynamical variable. Here we will be focused on the late time evolution of the universe. Now we assume the Taylor expansion of the scale factor around the current age  $t_0$  [59]:

$$(1 + z)^{-1} = \frac{a(t)}{a_0} = 1 + \sum_{n=1}^{\infty} \frac{A_n(t_0)}{n!} [H_0(t - t_0)]^2 \quad (11)$$

where  $A_n = \frac{a^n}{aH^n}$   $n \in N$ .  $a^n$  is the  $n^{th}$  derivative of the scale factor with respect to time. The deceleration parameter  $q \equiv -A_2$ ,  $A_3$ , has been known as the Statefinder ( $r$ ) [75] similar as the jerk ( $j$ ) [76].  $A_4$  is the snap ( $s$ ) and  $A_5$  is the lerk ( $l$ ) [77–79]. It is very surprising that, in a spatially flat universe, comprising of pressure less issue and a cosmological constant relate to the  $\Lambda$ CDM, while we shall represents all the parameters of  $A_n$  as the function of  $q$  and density

parameter  $\Omega_m$ . Likewise

$$\begin{aligned} A_2 &= 1 - \frac{3}{2}\Omega_m, \\ A_3 &= 1, \\ A_4 &= 1 - \frac{3^2}{2}\Omega_m, \\ A_5 &= 1 + 3\Omega_m + \frac{3^3}{2}\Omega_m^2, \\ A_6 &= 1 - \frac{3^3}{2}\Omega_m - 3^4\Omega_m^2 - \frac{3^4}{4}\Omega_m^3, \text{ etc.}, \end{aligned}$$

where  $\Omega_m = \frac{\Omega_{0m}(1+z)^3}{h^2(z)}$  and  $\Omega_m = \frac{2}{3}(1+q)$  is the concordance cosmology. It is interesting to note that the above expressions leads to define the Statefinder hierarchy  $S_n$ :

$$\begin{aligned} S_2 &= A_2 + \frac{3}{2}\Omega_m, \\ S_3 &= A_3, \\ S_4 &= A_4 + \frac{3^2}{2}\Omega_m, \\ S_5 &= A_5 - 3\Omega_m - \frac{3^3}{2}\Omega_m^2, \\ S_6 &= A_6 + \frac{3^3}{2}\Omega_m + 3^4\Omega_m^2 + \frac{3^4}{4}\Omega_m^3, \text{ etc.} \end{aligned}$$

The fundamental characteristic of this diagnostic, that all the  $S_n$  parameters remains fixed at unity for  $\Lambda$ CDM model while the astronomical development is going on.  $S_n|_{\Lambda\text{CDM}} = 1$  describe the null diagnostic for concordance cosmology.

## 4 Fractional Statefinder

The statefinder hierarchy equations produce a progression of diagnostic for  $\Lambda$ CDM model with  $n > 3$ . By using the relationship  $\Omega_m = \frac{2}{3}(1+q)$ , valid in  $\Lambda$ CDM. It is also possible to write Statefinders in an alternative form as:

$$\begin{aligned} S_3^{(1)} &= A_3, \\ S_4^{(1)} &= A_4 + 3(q+1), \\ S_5^{(1)} &= A_5 - 2(4+3q)(1+q), \text{ etc} \end{aligned}$$

It is clearly visible that in both of the methods yield identical results for  $\Lambda$ CDM:  $S_4^{(1)} = S_4$ ,  $S_5^{(1)} = S_5 = 1$ . However for other DE models, it is proposed that the two alternative definitions, of the state finder,  $S_n$  &  $S_n^{(1)}$ , would provide different results. It was shown in [55] that a second State finder could be used as  $S_3^{(1)} = S_3$

$$S_3^{(2)} = \frac{S_3^{(1)} - 1}{3(q - \frac{1}{2})} \quad (12)$$

In concordance cosmology  $S_3^{(1)} = 1$ , while  $S_3^{(2)}$  fix at zero. As a consequently the Statefinder pair  $(S_3^{(1)}, S_3^{(2)}) = (1, 0)$  for  $\Lambda$ CDM model. Similarly we characterize the second member of the Statefinder hierarchy as follows

$$S_n^{(2)} = \frac{S_n^{(1)} - 1}{\zeta(q - \frac{1}{2})}. \quad (13)$$

Here  $\zeta$  is the arbitrary constant.

In concordance cosmology  $S_n^{(2)} = 0$  for  $\Lambda$ CDM.  $\{S_n^{(1)}, S_n^{(2)}\} = \{1, 0\}$ . The second statefinder  $S_n^{(2)}$  helps in the desired aim of creating a break in some of the degeneracies present in  $S_n^{(1)}$ . We

give the specific expression of  $S_3^{(1)}$ ,  $S_3^{(2)}$ ,  $S_4^{(1)}$ ,  $S_4^{(2)}$  by using the variable  $\Omega_D$  and  $\omega_D$  depending on the redshift as

$$S_3^{(1)} = 1 + \frac{9}{2}\omega_D\Omega_D(1 + \omega_D) = 1 - \frac{9(\Delta - 2)\Delta(\Omega_D - 1)\Omega_D}{2((\Delta - 2)\Omega_D + 2)^2}, \quad (14)$$

$$S_3^{(2)} = 1 + \omega_D = 1 - \frac{\Delta}{(\Delta - 2)\Omega_D + 2}, \quad (15)$$

$$S_4^{(1)} = -\frac{1}{4}27(\omega_D + 1)(\omega_D\Omega_D)^2 + \frac{27}{2}\omega_D(\omega_D + 1)\left(\omega_D + \frac{7}{6}\right)\Omega_D + 1, \\ = \frac{-(43\Delta^3 - 141\Delta^2 + 102\Delta + 16)\Omega_D^3 + 6(12\Delta^3 - 43\Delta^2 + 34\Delta + 8)\Omega_D^2 - 3(9\Delta^3 - 39\Delta^2 + 34\Delta + 16)\Omega_D + 16}{2((\Delta - 2)\Omega_D + 2)^3}, \quad (16)$$

$$S_4^{(2)} = -\frac{1}{2}\omega_D(\omega_D + 1)\Omega_D - (\omega_D + 1)\left(\omega_D + \frac{7}{6}\right), \\ = -\frac{(\Delta - 2)(\Omega_D - 1)((2\Delta - 7)\Omega_D - 3\Delta + 7)}{3((\Delta - 2)\Omega_D + 2)^2}. \quad (17)$$

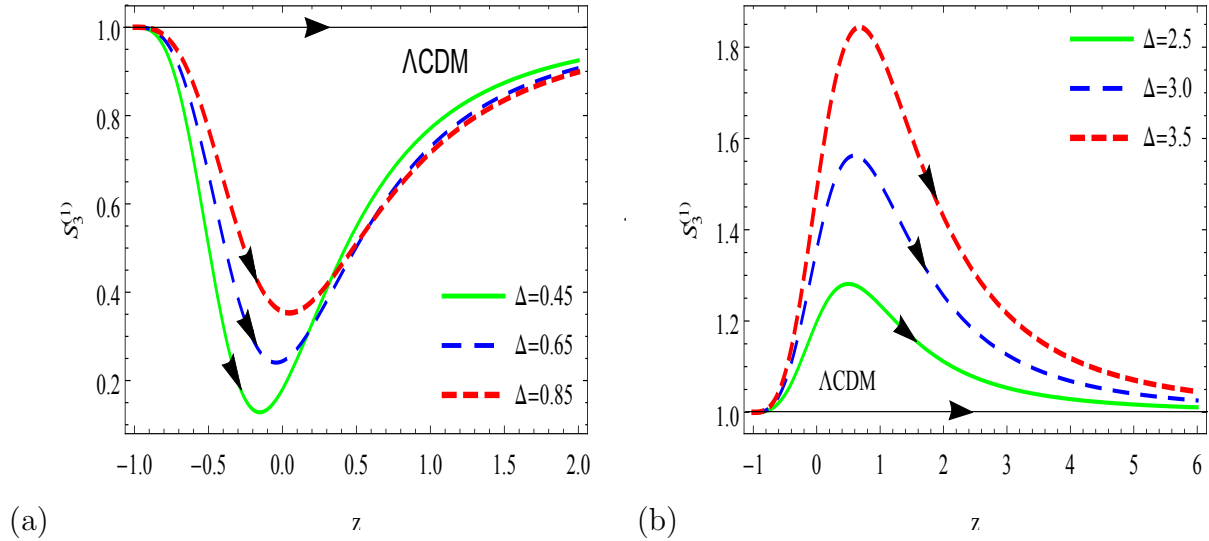


Figure 1: Evolution trajectories  $S_3^{(1)}$  verses  $z$  for different values of  $\Delta$

In Figures 1a & 1b, we plot the evolutionary trajectories of  $S_3^{(1)}$  verses redshift  $z$  for  $\Lambda BHDE$  model by using  $\Omega_{m_0} = 0.27$ ,  $C = 3$  and for different values of Barrow exponent  $\Delta$ . The curves associated with Barrow exponent  $\Delta$  and found a shape convex vertex below the  $\Lambda CDM$  line for  $\Delta < 2$  and also found a concave vertex shape in above the  $\Lambda CDM$  line by considering  $\Delta > 2$ . The curve has coincidence nature in fig 1a and 1b and again approaches towards the  $\Lambda CDM$ . From the figures 1a & 1b, we notice that  $S_3^{(1)}$  evolves decreasingly from 1 when  $\Delta < 2$  and  $S_3^{(1)}$  evolves increasing from 1 if  $\Delta > 2$ . All the curves of  $S_3^{(1)}(z)$  start below the  $\Lambda CDM$  line  $S_3^{(1)} = 1$  if  $\Delta < 2$  and crossing the  $\Lambda CDM$ , line for  $\Delta > 2$ . In order to draw a relevant comparison, the result of the  $\Lambda CDM$  model is represented additionally by a solid line. The curves of  $S_3^{(1)} = 1$  segregate well from  $\Lambda CDM$ .

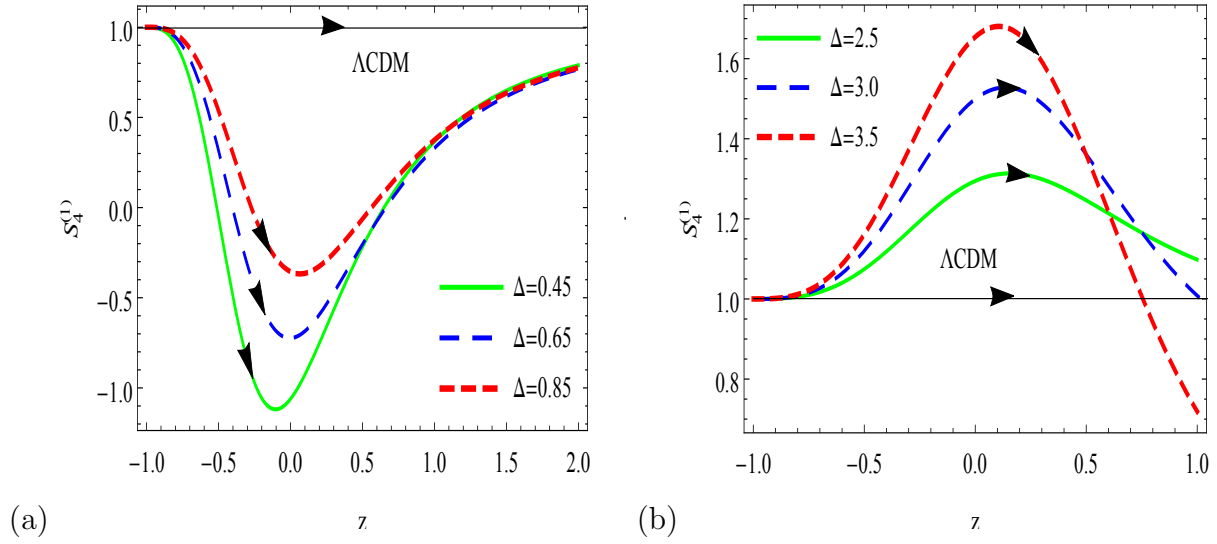


Figure 2: Evolution trajectories  $S_4^{(1)}$  verses  $z$  for different values of  $\Delta$

Figures 2a & 2b represent the evolutions of  $S_4^{(1)}$  versus redshift  $z$  for the different values of Barrow exponent  $\Delta$ . The figures depict the behaviour of BHDE and their results are compared with the  $\Lambda$ CDM line. The evolutionary trajectories of  $S_4^{(1)}$  show similar behaviour as of  $S_3^{(1)}$ . In Fig. 2a trajectories develop below the  $\Lambda$ CDM line ( $S_4^{(1)} = 1$ ) near the high redshift region and monotonically decreases then increases and finally tends to the  $\Lambda$ CDM for  $\Delta < 2$ . Fig. 2b depicts the trajectories of  $S_4^{(1)}$  for  $\Delta > 2$  above the  $\Lambda$ CDM line and form the concave vertex at high redshift. These trajectories are significantly separated and crossing the  $\Lambda$ CDM line.

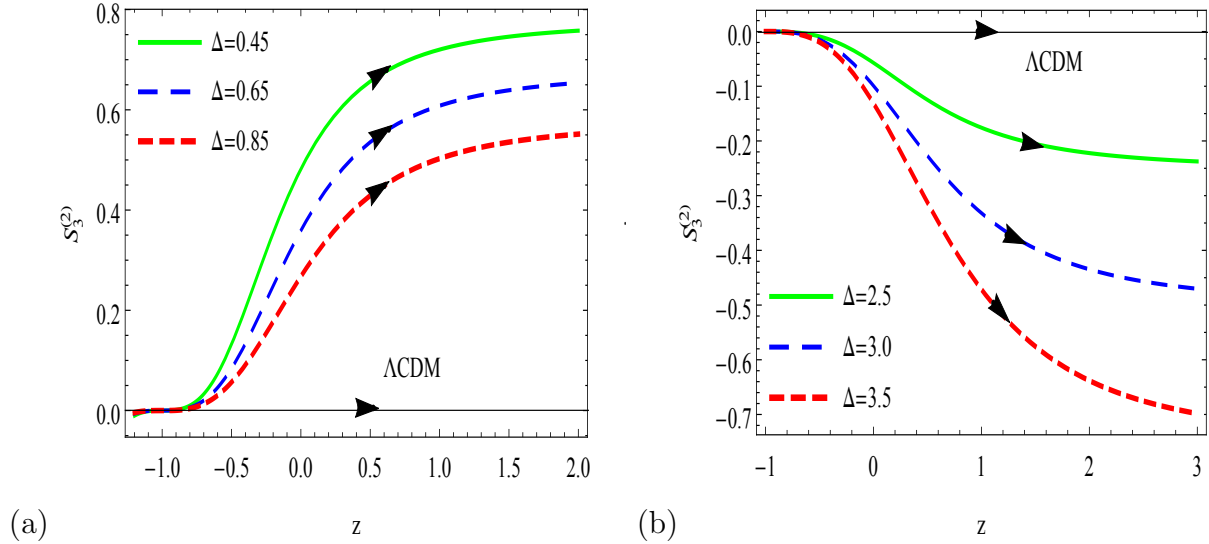


Figure 3: Evolution trajectories  $S_3^{(2)}$  verses  $z$  for different values of  $\Delta$

Figure 3a shows the evolutionary trajectories of  $S_3^{(2)}$  for the BHDE model for different values of parameter  $\Delta < 2$ . We observe that the evolutionary trajectories of  $S_3^{(2)}$  are distinct in themselves and can be differentiated from  $\Lambda$ CDM line  $S_3^{(2)} = 0$ , at high red-shift region for

$\Delta < 2$ . It evolves the  $\Lambda$ CDM line and separated well at high redshift. Similarly in Fig. 3b the trajectories evolve below the  $\Lambda$ CDM line and separated well in high redshift region, while at low redshift these trajectories degenerate closer together.

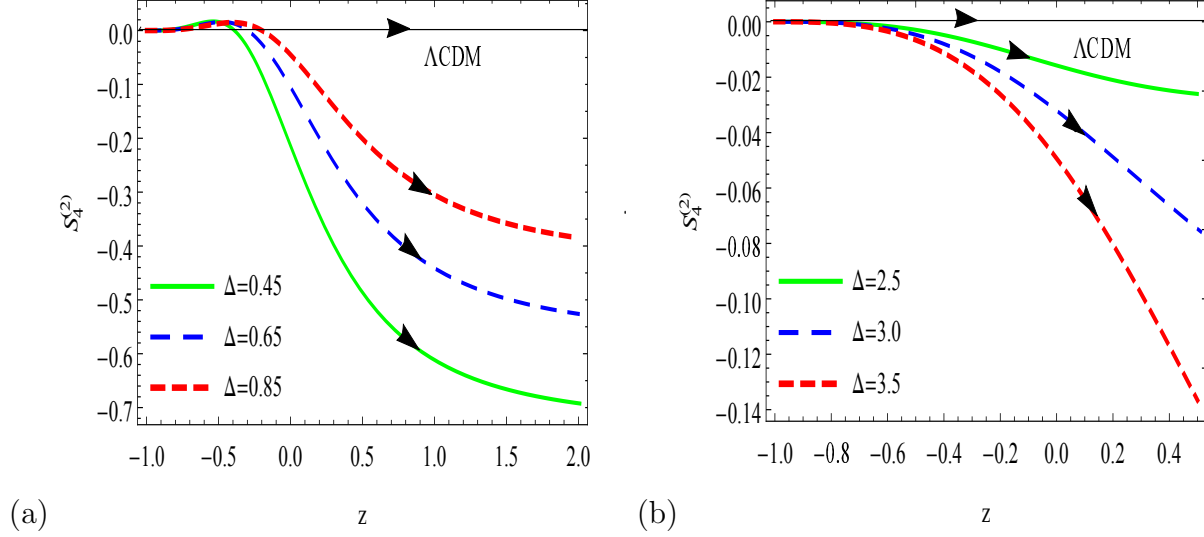


Figure 4: Evolution trajectories  $S_4^{(2)}$  versus  $z$  for different values of  $\Delta$

In Figures 4a & 4b the graphs show  $S_4^{(2)}$  evolution versus  $z$ . These figures are very much separated and evolve below the  $\Lambda$ CDM line  $S_4^{(2)} = 0$  at the high redshift. These transformative directions shows just quantitative effect on the  $S_4^{(2)}$  by fluctuating  $\Delta$  and at low redshift the trajectories degenerate closely together with  $\Lambda$ CDM.

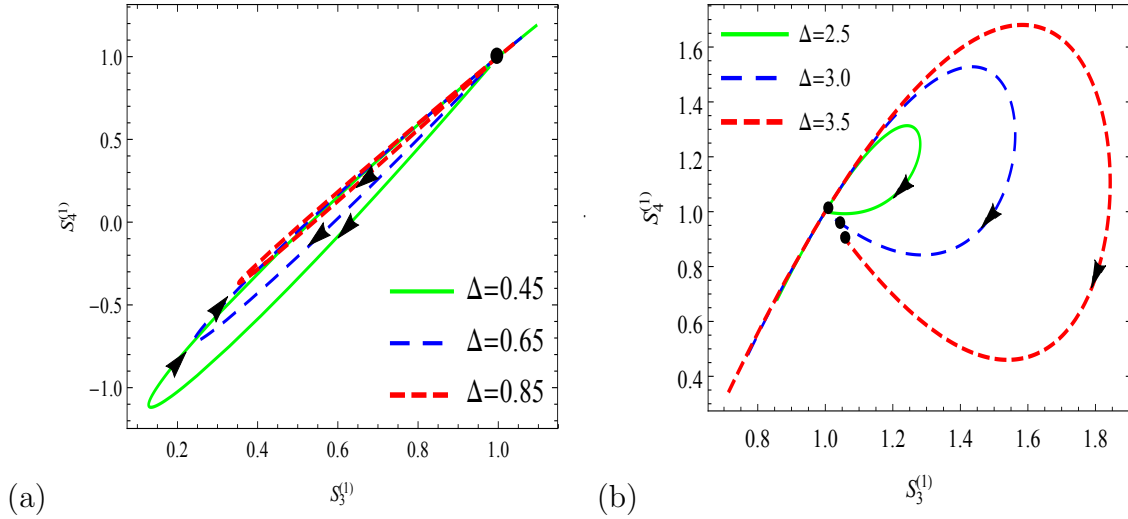


Figure 5: Evolution trajectories  $S_4^{(1)}$  versus  $S_3^{(1)}$  for different values of  $\Delta$

Figures 5a & 5b depict the Statefinders  $S_4^{(1)}$  and  $S_3^{(1)} \equiv S_3$  are expressed for BHDE model; the arrows and dots represent time evolution and present epoch respectively by using  $\Omega_{m0} = 0.27$ .  $\Lambda$ CDM relates to fixed point (1,1) for  $\Delta > 2$  and  $\Delta < 2$ .

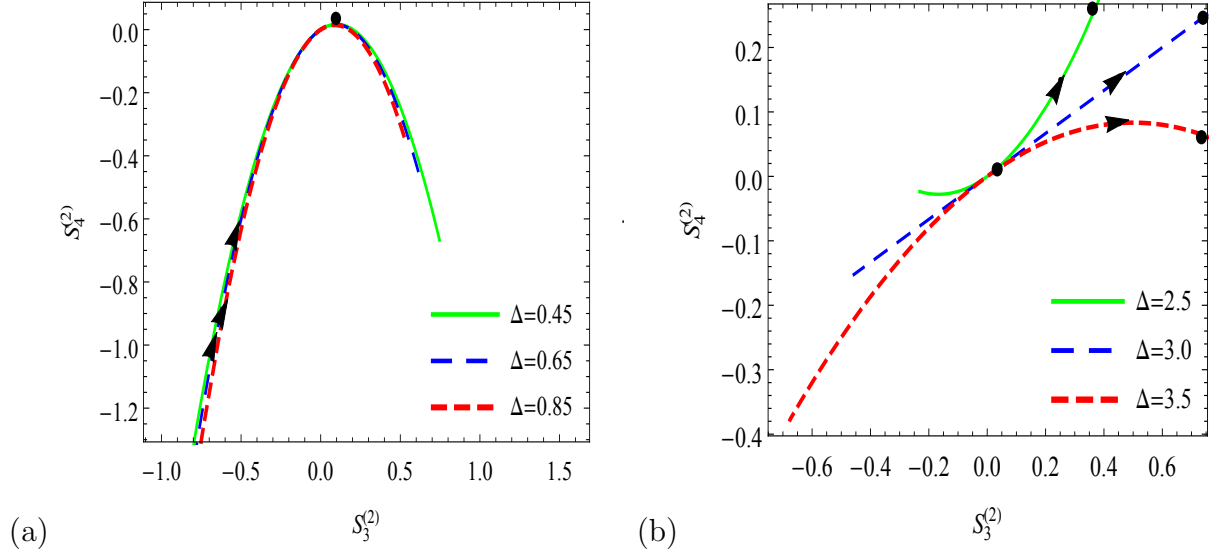


Figure 6: Evolution trajectories  $S_4^{(2)}$  versus  $S_3^{(2)}$  for different values of  $\Delta$

The Statefinders  $S_4^{(2)}$  and  $S_3^{(2)}$  are also shown in Figs. 6a & 6b for BHDE model. The fixed point at (0,0) in figure is  $\Lambda$ CDM. The arrows show time evolution furthermore, the current age in the various models is appeared as a dot by using  $\Omega_{m0} = 0.27$  for  $\Delta > 2$  and  $\Delta < 2$ . As we demonstrate in Figs. (1 – 6), the Statefinder hierarchy give us an incredible methods for recognizing dynamical DE models from  $\Lambda$ CDM.

## 5 Growth rate of perturbations

We use the "parametrized post-Friedmann" theoretical framework for the estimation of growth rate perturbations for the interaction of DE to acquire the  $\epsilon(z)$  values for the models numerically.

The perturbation growth rate parameter  $\epsilon$  [57, 58] is given by

$$\epsilon = \frac{f(z)}{f_{\Lambda\text{CDM}}(z)}, \quad (18)$$

where  $f(z) = \frac{d \log \delta}{d \log a}$  represents the structure's growth rate. Here,  $\delta = \frac{\delta_{\rho_m}}{\rho_m}$ , with  $\delta_{\rho_m} \rightarrow$  matter density perturbation,  $\rho_m \rightarrow$  energy density.

If the matter density perturbation is linear and there is no correlation between CDM and DE, the equation of late-time perturbation may be given as

$$\ddot{\delta} + 2H\dot{\delta} = 4\pi G\rho_m\delta, \quad (19)$$

where  $G \rightarrow$  gravitational constant. According for the linear density perturbation the growth rate is approximatively determined by [74]:

$$f(z) = \Omega_m(z)^\gamma, \quad (20)$$

$$\gamma = \frac{3}{5 - \frac{\omega}{1-\omega}} + \frac{3(1+\omega)(1 - \frac{3}{2}\omega)}{125(1 - \frac{6}{5}\omega)^3}(1 - \Omega_m(z)), \quad (21)$$

where  $\Omega_m(z) = \frac{\rho_m}{3H^2M_p^2}$  denotes the fractional density of matter. For example  $\gamma = 0.55$ , the above approximation follows the physical DE models well, when  $\omega$  is either a constant, or varies slowly for  $\Lambda$ CDM [74, 80].

In case of models other than this, the values taken up by  $\epsilon(z)$  display variations from  $\Lambda$ CDM for which the parameter keeping track of fractional growth is employed as a diagnostic. In the case of an interacting DE model, however, the growth rate can not be parametrized simply by Eqs. (20) and (21) [81].

This equation can be numerically solved for the condition  $f(z=0) = 1$  for the  $\Lambda$ CDM and the BHDE model. Depending on  $f(z)$ , other null diagnostic, known as fractional growth parameter  $\epsilon$ , is discussed in [56, 73].

## 5.1 Analysis of the composite null diagnostic

In this section, we have also introduced a composite null diagnostic (CND), which is a combination of members of state finder hierarchy and fractional growth parameter. This investigation of CND can be helpful to represent the conduct of geometrical and matter perturbation data of enormous development. In this paper, we use four CND pairs,  $(S_3^{(1)}, \epsilon)$  and  $(S_4^{(1)}, \epsilon)$ ,  $(S_3^{(2)}, \epsilon)$ , and  $(S_4^{(2)}, \epsilon)$  respectively. Initially we start the study of the fractional growth parameter  $\epsilon(z)$  to diagnose the  $\Lambda$ BHDE model. The evolutionary trajectories of  $(S_3^{(1)}, \epsilon)$  for BHDE model are plotted in figures 7a and 7b, where the current value of  $(S_3^{(1)}, \epsilon)$  is labeled with circular dots, and the fixed point  $S_3^{(1)} = (1, 1)$  for the  $\Lambda$ CDM model. It is also additionally appeared as a star for comparison. Figures 7a and 7b plot with  $S_3^{(1)}$  verses  $\epsilon$  for different values of  $\Delta$ . So we can use a composite null diagnostic (CND), as a combination of  $(S_3^{(1)}, \epsilon)$ . From the figure we noticed that, curve evolves near  $\Lambda$ CDM and monotonically decreases and forming convex vertices for  $\Delta < 2$  and for  $\Delta > 2$  it forms convex vertices and approaches to  $\Lambda$ CDM at high red shift. Figs. 7a and 7b show the evolutionary trajectories of  $(S_3^{(1)}, \epsilon)$  of BHDE model by considering various estimations of  $\Delta$ , where the star signifies the  $\Lambda$ CDM model of  $(S_3^{(1)}, \epsilon)$ .

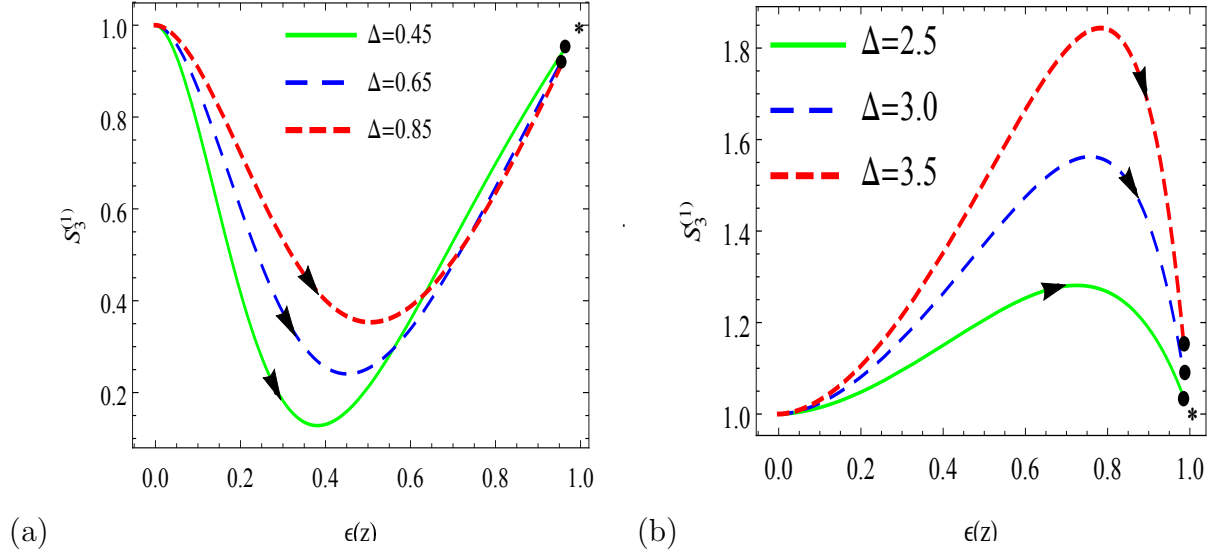


Figure 7: Evolution trajectories  $S_3^{(1)}$  versus  $\epsilon$  for different values of  $\Delta$

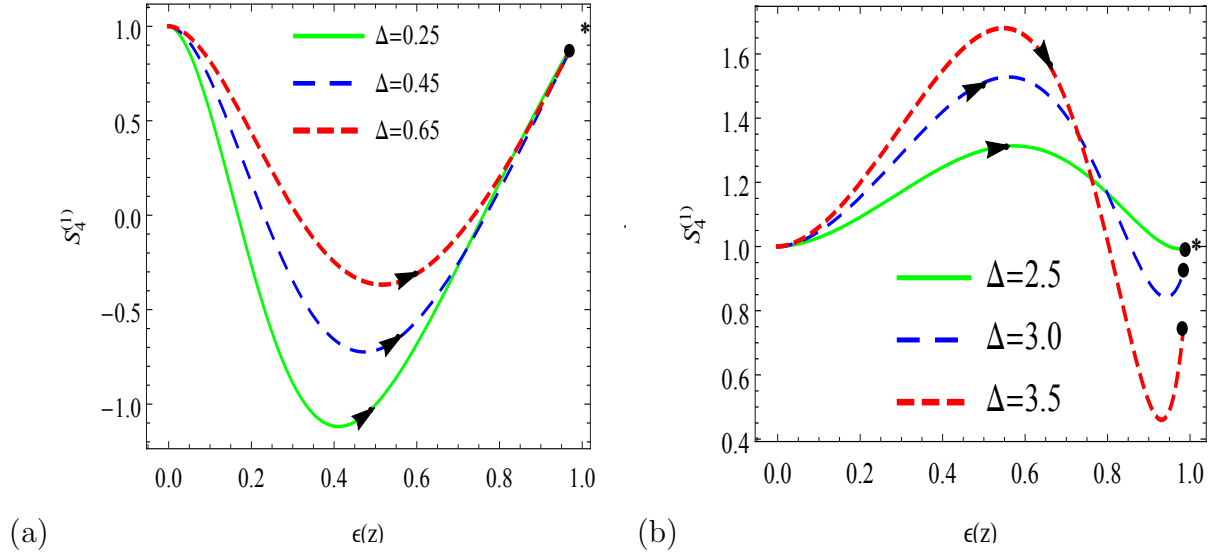


Figure 8: Evolution trajectories  $S_4^{(1)}$  versus  $\epsilon$  for different values of  $\Delta$

In addition, the CND ( $S_4^{(1)} - \epsilon$ ) is also used to study the BHDE model. We draw the evolutionary pathways for the Barrow holographic DE model. Figs. 8a & 8b show the present-day values of  $(S_4^{(1)}, \epsilon)$  and the fixed point  $(1, 1)$  for  $\Lambda$ CDM and direct measuring of effective distances between them. The evolutionary trajectories  $(S_4^{(1)} - \epsilon)$  forms the convex vertex for  $\Delta < 2$ . The current values of  $(S_4^{(1)}, \epsilon)$  for the BHDE are shown by dots. Similarly if we take  $\Delta > 2$  initially the curves form a concave vertex. The curves of CND pairs  $(S_4^{(1)}, \epsilon)$  show similar behavior of the curve  $(S_3^{(1)}, \epsilon)$ .

## 6 Conclusion

In this manuscript we have discussed the BHDE by utilizing the Barrow entropy, rather than the standard Bekenstein-Hawking. Our main focus in the manuscript is to diagnose BHDE model by the State finder hierarchy and composite null diagnostic (CND). The diagnostic tools which are frequently apply to test the DE models: (a) state finder hierarchy ( $S_3^{(1)}, \epsilon$ ) (b) fractional growth parameter  $\epsilon$ . Additionally the CND pair, are also considered to diagnosing DE models. So, the major concern of the work is to apply diagnostic tools for the BHDE models.

As per the following, the principal highlights of the models are :

- In Figures (1-6), the statefinder hierarchy gives the analytical expressions of  $S_3^{(1)}, S_4^{(1)}, S_3^{(2)}, S_4^{(2)}$  and elaborate numerically, for BHDE model. We have plotted the evolutionary curves of  $S_3^{(1)}, S_4^{(1)}, S_3^{(2)}, S_4^{(2)}$  with respect to the redshift  $z$  and  $\epsilon(z)$ . The evolutionary trajectories of  $S_3^{(1)}, S_4^{(1)}$  evolve below the  $\Lambda$ CDM line and form the convex vertex for the barrow exponent  $\Delta < 2$  while  $S_3^{(2)}, S_4^{(2)}$  expand from above the  $\Lambda$ CDM line and form the concave vertex for  $\Delta > 2$ .
- We have also examined the the trajectories ( $S_3^{(1)}, \epsilon$ ) and ( $S_4^{(1)}, \epsilon$ ) for BHDE. Evolutionary trends have similar approach as shown in Figs. (7) – (8). In contrast, we have assumed the various values of  $\Delta$  showing qualitative impacts on  $\Lambda$ BHDE. We conclude that the diagnostic tools are efficiently applicable to distinguished BHDE models. Furthermore,  $S_4^{(1)}$  can generally predict larger variation amongst the cosmic evolution of the BHDE in comparison to  $S_3^{(1)}$ . In this way we get an easier approach to distinguish different theoretical models.
- In addition, as compared with  $S_3^{(1)}, S_4^{(1)}$  and  $\epsilon(z)$ , CND pairs have substantially distinct evolutionary routes. They are more effective in diagnosing different theoretical models of DE. It implies that CND will provide the state with a great supplement At the same time, the statefinder hierarchy and the cosmological data of structure growth rate were obtained by the CND process.
- Thus the above study concludes that the BHDE and  $\Lambda$ CDM models can be easily differentiated by considering state finder for different parametric values.

In summary, by using these diagnostic methods, we can conclude that the BHDE model can be easily differentiated.

## Acknowledgments

The authors are thankful to Dr. Kasturi Sinha Ray (GLA University) for her help in preparing the manuscript.

# References

- [1] A. G. Riess *et al.*, Observational evidence from supernovae for an accelerating universe and cosmological constant, *Astron. J.* **116** (1998) 1009.
- [2] S. Perlmutter *et al.*, Measurements of omega and lambda from 42 high-redshift supernovae, *Astrophys. J.* **517** (1999) 565.
- [3] D. N. Spergel *et al.*, First year Wilkinson Microwave Anisotropy Probe (WMAP) observations: Determination of cosmological parameters, *Astrophys. J. Suppl.* **148** (2003) 175, [astro-ph/0302209].
- [4] M. Tegmark *et al.*, Cosmological parameters from SDSS and WMAP, *Phys. Rev. D* **69** (2004) 103501, [astro-ph/0310723].
- [5] M. Li and R. X. Miao, A New Model of Holographic Dark Energy with Action Principle, arXiv:1210.0966 [hep-th].
- [6] H. Wei and R. G. Cai, A New Model of Holographic Dark Energy, *Phys. Lett. B* **660** (2008) 113.
- [7] C. Gao, F. Q. Wu, X. Chen and Y. G. Shen, A Holographic Dark Energy Model from Ricci Scalar Curvature, *Phys. Rev. D* **79** (2009) 043511, arXiv:0712.1394.
- [8] X. Zhang, Heal the world: Avoiding the cosmic doomsday in the holographic dark energy model, *Phys. Lett. B* **683** (2010) 81, arXiv:0909.4940.
- [9] J. F. Zhang, M. M. Zhao, J. L. Cui and X. Zhang, Revisiting the holographic dark energy in a non-at universe: alternative model and cosmological parameter constraints, *Eur. Phys. J. C* **74** (2014) 3178, [arXiv:1409.6078].
- [10] B. Ratra and P. J. E. Peebles, Cosmological consequences of a rolling homogeneous scalar field, *Phys. Rev. D* **37** (1988) 3406.
- [11] P. J. E. Peebles and B. Ratra, Cosmology with a time variable cosmological constant, *Astrophys. J.* **325** (1988) L17 .
- [12] X. Zhang, Reconstructing holographic quintessence, *Phys. Lett. B* **648** (2007) 1, [astro-ph/0604484].
- [13] J. F. Zhang, X. Zhang and H. Y. Liu, Reconstructing generalized ghost condensate model with dynamical dark energy parametrizations and observational datasets, *Mod. Phys. Lett. A* **23** (2008) 139, [astro-ph/0612642].
- [14] X. Zhang, Dynamical vacuum energy, holographic quintom and the reconstruction of scalar-field dark energy, *Phys. Rev. D* **74** (2006) 103505, [astro-ph/0609699].
- [15] R. Bousso, The holographic principle for general backgrounds, *Class. Quantum Grav.*, **17** (2000) 997.
- [16] A. De Felice and S. Tsujikawa,  $f(R)$  theories, *Living Rev. Rel.* **13** (2010) 3, arXiv:1002.4928.

- [17] S. Nojiri and S. D. Odintsov, Dark energy, inflation and dark matter from modified  $F(R)$  gravity, *TSPU Bulletin* **8** (2011) 7, arXiv:0807.0685.
- [18] T. Paul, Holographic correspondence of  $F(R)$  gravity with/without matter fields, *Europhys. Lett.* **127**, (2019) 20004.
- [19] G. R. Dvali, G. Gabadadze and M. Porrati, 4-D gravity on a brane in 5-D Minkowski space, *Phys. Lett. B* **485** (2000) 208, hep-th/0005016.
- [20] E. J. Copeland, M. Sami and S. Tsujikawa, Dynamics of dark energy, *Int. J. Mod. Phys. D* **15** (2006) 1753, [hep-th/0603057].
- [21] V. Sahni and A. A. Starobinsky, Reconstructing dark energy, *Int. J. Mod. Phys. D* **15** (2006) 2105, [astro-ph/0610026].
- [22] M. Kamionkowski, Dark matter and dark energy, arXiv:0706.2986 [astro-ph].
- [23] M. Li, X. D. Li, S. Wang and Y. Wang, Dark energy, *Commun. Theor. Phys.* **56** (2011) 525, [arXiv:1103.5870].
- [24] M. Li, X. D. Li, S. Wang, and Y. Wang, Dark energy: A brief review, *Front. Phys.* **8** (2013) 828..
- [25] J. A. Frieman , S. M. Turner and D. Huterer, Dark energy and the accelerating universe, *Ann. Rev. Astron. Astrophys.* **46** (2008) 385.
- [26] R. R. Caldwell, M. Kamionkowski and N. N. Weinberg, Phantom energy: Dark energy with  $\omega < -1$  causes a cosmic doomsday, *Phys. Rev. Lett.* **91** (2003) 071301.
- [27] B. Feng, X. L. Wang and X. M. Zhang, Dark energy constraints from the cosmic age and supernova, *Phys. Lett. B* **607** (2005) 35.
- [28] H. Wei, R. G. Cai and D. F. Zeng, Hessian: a new view of quintom dark energy, *Class. Quant. Grav.* **22** (2005) 3189.
- [29] T. Y. Xia and Y. Zhang, 2-loop quantum Yang–Mills condensate as dark energy, *Phys. Lett. B* **656** (2007) 19.
- [30] S. Wang and Y. Zhang, Alleviation of cosmic age problem in interacting dark energy model, *Phys. Lett. B* **669** 201 (2008).
- [31] G. 't Hooft, Dimensional reduction in quantum gravity, arXiv:gr-qc/9310026 (1993).
- [32] L. Susskind, The world as a hologram, *J. Math. Phys.* **36** (1995) 6377.
- [33] M. Li, A model of holographic dark energy, *Phys. Lett. B* **603** (2004) 1.
- [34] Q. G. Huang, M. Li, X. D. Li and S. Wang, Fitting the constitution type Ia supernova data with the redshift-binned parametrization method, *Phys. Rev. D* **80** 083515 (2009).
- [35] S. Wang, X. D. Li and M. Li, Revisit of cosmic age problem, *Phys. Rev. D* **82** (2010) 103006.

- [36] X. D. Li, S. Li, S. Wang, W. S. Zhang, Q. G. Huang and M. Li, Probing cosmic acceleration by using the SNLS3 SNIa dataset, *JCAP* **1107**, (2011) 011.
- [37] J. L. Cui, Y. Y. Xu, J. F. Zhang and X. Zhang, Strong gravitational lensing constraints on holographic dark energy, *Sci. China Phys. Mech. Astron.* **58** (2015) 110402.
- [38] D. Z. He and J. F. Zhang, Redshift drift constraints on holographic dark energy, *Sci. China Phys. Mech. Astron.* **60** (2017) 039511.
- [39] S. Wang, Y. Z. H, and M. Li, Cosmological implications of different baryon acoustic oscillation data, *Sci. China-Phys. Mech. Astron.* **60** (2017) 040411, arXiv: 1506.08274.
- [40] A. Pradhan, A. Dixit and S. Singhal, Anisotropic MHRDE model in BD theory of gravitation, *Int. J. Geom. Methos Mod. Phys.* **16** (2019) 1950185.
- [41] Shinichi Nojiri, S. D. Odintsov, V. K. Oikonomou, Tanmoy Paul, Unifying holographic inflation with holographic dark energy: a covariant approach, *Phys. Rev. D* **102** (2020) 023540, arXiv: 2007.06829 [gr-qc].
- [42] M. Tavayef, A. Sheykhi, K. Bamba, H. Moradpour, Tsallis holographic dark energy, *Phys. Lett. B* **781** (2018) 195.
- [43] A. Dixit, U. K. Sharma and A. Pradhan, Tsallis holographic dark energy in FRW universe with time varying deceleration parameter, *New Astronomy* **73** (2019) 101281.
- [44] M. Abdollahi Zadeh, A. Sheykhi, H. Moradpour, Tsallis agegraphic dark energy model, *Mod. Phys. Lett. A* **34** (2019) 1950086.
- [45] H. Moradpour, S. Moosavi, I. Lobo, J. Morais Graca, A. Jawad, I. Salako, Thermodynamic approach to holographic dark energy and the Renyi entropy, *Eur. Phys. J. C* **78** (2018) 829.
- [46] A. Dixit, V. K. Bhardwaj and A. Pradhan, RHDE model in FRW Universe with two IR cut-offs with redshift parametrization, *Europ. Phys. J. Plus* **135** (2020) 831.
- [47] A. Sayahian Jahromi *et.al.*, Generalized entropy formalism and a new holographic dark energy model, *Phys. Lett. B* **780** (2018) 21.
- [48] V. C. Dubey, U. K. Sharma and A. Pradhan, Sharma-Mittal holographic dark energy model in conharmonically flat space-time, *Int. J. Geom. Methos Mod. Phys.* **18** (2021) 2150002.
- [49] S. Nojiri, S. D. Odintsov, E. N. Saridakis, Modified cosmology from extended entropy with varying exponent, *Eur. Phys. J. C* **79** (2019) 242.
- [50] Q. Huang, H. Huang, J. Chen, L. Zhang, F. Tu, Stability analysis of a Tsallis holographic dark energy model, *Class. Quant. Grav.* **36** (2019) 175001.
- [51] S. Ghaffari, H. Moradpour, I. P. Lobo, J. P. Morais Graaa, V. B. Bezerra, Tsallis holographic dark energy in the Brans–Dicke cosmology, *Eur. Phys. J. C* **78(9)** (2018) 706.
- [52] E. N. Saridakis, K. Bamba, R. Myrzakulov, F. K. Anagnostopoulos, Holographic dark energy through Tsallis entropy, *JCAP* **1812** (2018) 012.

- [53] S. Ghaffari, H. Moradpour, V. B. Bezerra, J. Morais Graaa, I. Lobo, Tsallis holographic dark energy in the brane cosmology, *Phys. Dark Univ.* **23** (2019) 100246.
- [54] S. Srivastava, U. K. Sharma, A. Pradhan, New holographic dark energy in Bianchi-III universe with k-essence, *New Astronomy* **68** (2019) 57.
- [55] V. Sahni, T.D. Saini, A. A. Starobinsky, U. Alam, Statefinder-a new geometrical diagnostic of dark energy, *J. Exp. Theo. Phy. Lett.* **77** , (2003) 201, arXiv:astro-ph/0201498.
- [56] M. Arabsalmani and V. Sahni, Statefinder hierarchy: An extended null diagnostic for concordance cosmology, *Phys. Rev. D* **83** (2011) 043501.
- [57] V. Acquaviva, A. Hajian, D. N. Spergel and S. Das, Next generation redshift surveys and the origin of cosmic acceleration, *Phys. Rev. D* **78** (2008) 043514.
- [58] V. Acquaviva and E. Gawiser, How to falsify the GR+ $\Lambda$ CDM model with galaxy redshift surveys, *Phys. Rev. D* **82** (2010) 082001.
- [59] F. Yu, J. L. Cui, J. F. Zhang and X. Zhang, Statefinder hierarchy exploration of the extended Ricci dark energy, *Eur. Phys. J. C* **59** (2013) 274.
- [60] E. N. Saridakis, Barrow holographic dark energy, arXiv: 2005.04115 (2020).
- [61] A. Pradhan, A. Dixit and V. K. Bhardwaj, Barrow HDE model for Statefinder diagnostic in FLRW Universe, *Int. J. Mod. Phys. A* Accepted (2021), arXiv:2101.00176[gr-qc].
- [62] J. D. Barrow, The area of a rough black hole, *Phys. Lett. B* **808** (2020).
- [63] S. N. Saridakis, S. Basilakas, The generalized second law of thermodynamics with Barrow entropy, arXiv: 2005.08258[gr-qc] (2000).
- [64] F. K. Anagnostopoulos, S. Basilakos and E. N. Saridakis, Observational constraints on Barrow holographic dark energy, arXiv: 2005.10302 (2020).
- [65] J. D. Barrow S. Basilakos and E. N. Saridakis, Big Bang Nucleosynthesis constraints on Barrow entropy, *Phys. Lett. B* (2021) 136134, <https://doi.org/10.1016/j.physletb.2021.136134>, [arXiv:2010.00986].
- [66] S. Wang, Y. Wang and M. Li, Holographic dark energy, *Phys. Rept.* **696** (2017) 1.
- [67] S. Srivastava, U. K. Sharma, Barrow holographic dark energy with Hubble horizon as IR cutoff, arXiv: 2010.09439[physics.gn-ph] (2020).
- [68] A. A. Mamon, A. Paliathanasis, S. Saha, Dynamics of an interacting Barrow holographic dark energy model and its thermodynamic implications, arXiv: 2007.16020[gr-qc] (2000).
- [69] E. M. C. Abreu, J. A. Neto, Barrow black hole corrected-entropy model and Tsallis nonextensivity, *Phys. Lett. B* **810**, (2020), 135805.
- [70] E. M. C. Abreu, J. A. Neto, Barrow fractal entropy and the black hole quasinormal modes, *Phys. Lett. B* **807**, (2020), 135602.

- [71] E. N. Saridakis, Modified cosmology through spacetime thermodynamics and Barrow horizon entropy, *JCAP* **07** (2020) 031, arXiv:2006.01105.
- [72] L. Zhou and S. Wang, Diagnosing  $\Lambda$ HDE model with statefinder hierarchy and fractional growth parameter, *Sci. China Physics, Mechanics and Astronomy* **59** (2016) 670411.
- [73] Z. Zhao and S. Wang, Diagnosing holographic type dark energy models with the Statefinder hierarchy, composite null diagnostic and  $\omega - \omega'$  pair, *Sci. China Physics, Mechanics & Astronomy* **61** (2018) 039811.
- [74] L. M. Wang and P. J. Steinhardt, Cluster abundance constraints on quintessence models, *Astrophys. J.* **508** (1998) 483 [astro-ph/9804015].
- [75] T. Chiba and T. Nakamura, The luminosity distance, the equation of state, and the geometry of the universe, *Prog. Theor. Phys.* **100** (1998) 1077.
- [76] M. Visser, Jerk, snap and the cosmological equation of state, *Classical Quantum Gravity* **21** (2004) 2603.
- [77] M. P. Dabrowski, Statefinders, higher-order energy conditions, and sudden future singularities, *Phys. Lett. B* **625** (2005) 184.
- [78] S. Capozziello, V. F. Cardone, and V. Salzano, Cosmography of  $f(R)$  gravity, *Phys. Rev. D* **78** (2008) 063504.
- [79] M. Dunajski and G. Gibbons, Cosmic jerk, snap and beyond, *Classical Quantum Gravity* **25** (2008) 235012.
- [80] E. V. Linder, Cosmic growth history and expansion history, *Phys. Rev. D* **72** (2005) 043529 [astro-ph/0507263].
- [81] G. Caldera-Cabral, R. Maartens and B. M. Schaefer, The growth of structure in interacting dark energy models, *JCAP* **0907** (2009) 027, arXiv:0905.0492 [astro-ph.CO].